ACS OMEGA

http://pubs.acs.org/journal/acsodf

Article

Kaolin-Supported Silver Nanoparticles as an Effective Catalyst for the Removal of Methylene Blue Dye from Aqueous Solutions

Zinabu Gashaw Asmare, Belete Asefa Aragaw,* Minaleshewa Atlabachew,* and Tessera Alemneh Wubieneh

Cite This: *ACS Omega* 2023, 8, 480−491

Read Online

ACCESS | Metrics & More | Article Recommendations

ABSTRACT: Water contamination by organic dyes has become a reason for severe environmental pollution and has been threatening the aquatic ecosystem. In this study, kaolin-supported silver nanoparticle (Ag-NP) composites were synthesized by a facile two-step adsorption−reduction method through the reduction of silver ions adsorbed onto locally available, inexpensive, and easily pretreated kaolin surfaces by using sodium borohydride ($NaBH_4$) for the catalytic degradation of methylene blue (MB) dye in aqueous solution. The morphology, structure, surface area, and interaction of the synthesized materials were investigated by scanning electron microscopy, X-ray diffraction, Brunauer−Emmett−Teller, and Fourier transform infrared spectroscopy, respectively. Characterization results showed the successful growth of Ag-NPs on the kaolin surface. To understand the catalytic degradation performance of the catalyst, batch experiments were carried out using MB dye as a model dye. The catalytic reduction tests confirmed the importance of Ag-NPs and the high catalytic activities of the synthesized Ag-NPs/kaolin composite toward MB dye reduction. The degradation results indicated that the increased Ag-NP content on the kaolin surface through repeating cycles could effectively enhance the removal of MB dye from an aqueous solution. The kinetic analysis of the MB dye degradation of the catalyst has fitted the pseudo-first-order kinetic model. More than 97% removal efficiency was still present after five reuse cycles, demonstrating exceptional stability and reusability of the composite. In conclusion, the Ag-NPs supported kaolin (Ag-NPs/kaolin) composite was found to be a promising catalyst for the excellent catalytic activity to reduce a model dye MB from the aqueous solution in the presence of $NaBH_4$ with catalytic efficiency higher than 97% and a reduction rate constant, k_{red}, higher than 0.86 min^{-1}.

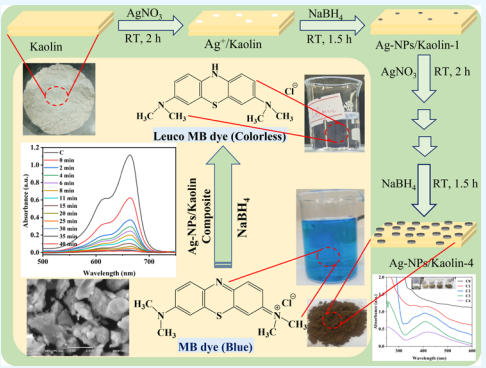

1. INTRODUCTION

Nowadays, severe global environmental pollution has been threatening the ecosystem and human health worldwide by contaminating soil and water.[1] Various contaminant effluents, including organic dyes, chlorinated compounds, heavy metals, soaps, detergents, surfactants, salts, and inhibitory compounds that are released from food, pharmaceutical, cosmetics, paints, plastics, textile, paper, leather, and other industries into water bodies are the primary source of water pollution and which, in turn, induces water resource shortage.[2−7] Among these pollutants, organic dyes are the most difficult-to-treat constituents of industrial effluents because of their complicated chemical structure, high solubility, and nonbiodegradability.[8,9] These organic dyes can pollute the water body, enter the human body through the food chain, and cause many dangerous diseases like skin irritation, permanent blindness, hypertension, vertigo, vomiting gastritis, and even mutation or cancer.[10,11] In addition, the release of these colored materials (for example, methylene blue (MB) dye) into water bodies can interfere with photosynthesis and oxygen exchange capacity, which leads to severe damage to aquatic organisms by hindering the infiltration of sunlight.[11] Removing dye molecules from water sources has therefore become a primary environmental concern and a challenge.[12]

Various conventional water treatment techniques have been used for organic dyes, including coagulation, filtration, adsorption, biodegradation, ultrafiltration, chemical, photochemical, electrochemical, and reverse osmosis method removal. Nevertheless, removing these organic dyes from water is difficult because of their aromatic structural stability.[13] In recent years, nanocatalysis has emerged as an alternative to conventional water treatment methods. The finite size, large surface-to-volume ratio, and size-dependent reactivity have

Received: August 16, 2022
Accepted: December 14, 2022
Published: December 26, 2022

made metal nanoparticles an efficient catalyst.[14] Nowadays, nanocatalysts are one of the promising materials for removing organic dyes from industrial effluents before discharge into our water resources.[15]

Previously, the application of silver nanoparticles (Ag-NPs) as a catalyst for water purification, such as efficient catalytic removal of organic dyes, has been widely reported due to its fascinating characteristics and substantial catalytic potential.[16−21] When pure nanoparticles are used alone, the easy aggregation between nanoparticles will impede their catalytic activity and practical application.[22−25] Several studies reported that aggregation of nanoparticles could be prevented by growing nanoparticles on support materials.[9,16−18,26,27] However, most of the support/carrier materials are expensive, and the synthesis processes are complex and time-consuming. One of the most efficient agglomeration solutions with the least cost is synthesizing nanoparticles based on clay compounds as the support material. The nanoparticles are maintained within the interlamellar spaces of clay and on its external surfaces.[28−33]

Clays have gained significant attention in material science due to their inherent properties, such as high surface area, good swelling, adsorption behavior, and ion exchange capacity.[34,35] Moreover, it is known that using clays to support Ag-NPs can amplify the electrochemical signal of the bare nanoparticles,[36,37] an essential property for the production of sensors for different applications. Recently, clay minerals as nanoparticle supports have been attracting significant attention due to their environmental and economic advantages in comparison with many other support materials such as graphene and carbon nanotubes.[28,38]

Kaolin, one of the common clay minerals, has been studied as a nanoparticle support due to its low cost, abundance, and eco-friendliness.[22,39−41] In particular, its exceptional properties, such as high versatility and thermal and mechanical stability, make it essential to act as a nanocatalyst support.[42,43] Kaolin is a phyllosilicate material and presents a nanolayered structure. The layers composing kaolinite's primary particles are stacked together by van der Waals and electrostatic forces. Each layer comprises a tetrahedral sheet condensed with a single octahedral sheet into one unit layer.[44,45] Because of its layered structure, kaolinite can be easily modified to produce hybrids and composites.[40,46−48] Silver nanoparticles are prepared by reducing silver nitrate ($AgNO_3$) with biological or chemical reduction methods.[49] One drawback of biological methods is that they are slow compared to chemical methods.[50] A chemical reduction method is usually applied to fabricate the Ag-based composites in the presence of reductants such as hydrazine, sodium borohydride ($NaBH_4$), sodium citrate ($Na_3C_6H_5O_7$), and dopamine ($C_8H_{11}NO_2$).[51−54]

Thus, in the current work, the Ag-NPs/kaolin composite was synthesized using an aqueous $NaBH_4$ as a reducing agent at room temperature with an efficient, low-cost, simple, and rapid one-pot solution-based route. The cationic silver compound $AgNO_3$ was used as a precursor. Kaolin has been used as a support material to synthesize a heterogeneous catalyst. Microscopy, spectroscopy, and other methods were used to characterize the resulting samples. The catalytic activity of the synthesized Ag-NPs/kaolin composite was determined against MB degradation in aqueous solution in the presence of $NaBH_4$. The synthesized catalyst exhibited excellent catalytic activity and could be reused for multiple catalytic cycles without any appreciable loss in its efficiency.

2. MATERIALS AND METHODS

2.1. Materials. The kaolin clay, used as a solid supporter for the Ag-NPs, was collected from Gasay, South Gondar Zone, Amhara Region, Ethiopia. The clay mineral was dried under dry conditions. Silver nitrate ($AgNO_3$, 99.999%, unichem chemical), sodium borohydride ($NaBH_4$, 97%, Savgan Heights plc), and methylene blue (MB, $C_{16}H_{18}ClNS$, Dallul Pharmaceuticals plc) were of analytical grade and used as received without further purification. Deionized water was used in the preparation of all solutions.

2.2. Synthesis Technique. *2.2.1. Wet Beneficiation of Kaolin Clay.* First, the raw kaolin clay was crushed and ground using a mortar and pestle to produce fine powder and sieved by a 75 μm sieve. Then, the powder was subjected to beneficiation (wet treatment) using deionized water. The beneficiation step is crucial to remove physically and chemically combined impurities like metallic oxide, soluble salts, organic matter, quartz, grits, and generally coarse particles to make an elegant powder.[55−57] This was done by soaking 100 g of finely powdered kaolin in 1 L of deionized water and stirring under a magnetic stirrer for 24 h at room temperature. The mixture was allowed to settle until a solid cake-like clay was obtained, and the solid cake-like clay was separated by filtration and washed with deionized water three times. Then, the obtained solid product was dried in an oven at 60 °C overnight. Finally, the dried product was ground and sieved for further use.

2.2.2. Synthesis of Ag-NPs/Kaolin Composites. A weighed mass of 5 g of beneficiated kaolin powder was dispersed in 100 mL of deionized water and stirred for about 30 min with a magnetic stirrer. Afterward, the mixture was allowed to settle, and the solid part was separated by filtration. Exactly 100 mL of silver nitrate solution (5 mM) was added into the suspension and stirred for 2 h. The suspension was then allowed to settle, and the solid product was separated by filtration. The surface of the suspension was washed with deionized water two to three times to remove the silver ion residue. Then, 100 mL of sodium borohydride (20 mM) was added to the suspension under stirring for 1.5 h. The solid product was separated by filtration and washed with deionized water until the yellow color in the filtrate disappeared. The obtained residue was dried in an air oven at 60 °C overnight. The resultant composite was named the first cycle and collected for the subsequent work. These procedures were repeated four times, following the same path for further comparison. Still, the mass of kaolinite varies approximately by 1 g, and $AgNO_3$ and $NaBH_4$ solution were reduced by 20 mL for each successive cycle to control the size of Ag-NPs. The four products are named as Ag-NPs/kaolin composite-1, Ag-NPs/kaolin composite-2, Ag-NPs/kaolin composite-3, and Ag-NPs/kaolin composite-4. Scheme 1 shows the synthesis mechanism of Ag-NPs onto the kaolin surface using $NaBH_4$ as the reductant.

Scheme 1. In Situ Synthesis of Ag-NPs Supported on the Kaolin Surface by Soaking in $AgNO_3$ Solution and Reducing using $NaBH_4$ as the Reductant

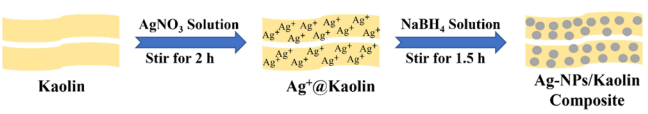

https://doi.org/10.1021/acsomega.2c05265
ACS Omega 2023, 8, 480−491

2.3. Characterization Techniques. X-ray diffraction (XRD) patterns of kaolin and Ag-NPs/kaolin composite powders were performed on an XRD-7000 X-ray diffractometer (Shimadzu, Japan) using Cu Kα radiation (λ = 0.15406 nm) at a 40 kV generator voltage and 30 mA generator current. The scanned 2θ range was from 10° to 80°, and the scanning rate was 3°/min. The UV absorption spectra were obtained on a Cary 60 UV−vis spectrophotometer (Agilent Technologies, Santa Clara, California, USA). Fourier transform infrared (FT-IR) spectra were recorded on an FT/IR-6600 FT-IR spectrometer (JASCO International Co., Ltd., Tokyo, Japan) between 4000 and 400 cm^{-1}. Brunauer−Emmett−Teller (BET) surface area, pore volume, and pore size measurements were done using Quantachrome NovaWin-Data Acquisition and Reduction for NOVA instruments 1994−2010, Quantachrome Instruments version 11.0 at 77.3 K. The BET model determined the surface areas of beneficiated kaolin and Ag-NPs/Kaolin composite according to the BET isotherm at a P/P_0 ratio from 0.0458 to 0.297. The samples were exposed to an overnight drying process at 90 °C to eliminate any volatile moisture and pollutants that had been adsorbed. Scanning electron microscopy (SEM) images were observed by JEOL NeoScope JCM-6000Plus Benchtop SEM (HITACHI, Japan) at accelerating voltages of 10 and 15 kV.

2.4. Catalytic Performance of Ag-NPs/Kaolin Composites on MB Dye. To investigate the catalytic performance of the synthesized Ag-NPs/Kaolin composites, the reduction efficiency of MB dye in an aqueous solution was measured in the presence of $NaBH_4$. Generally, 5 mg of the required composite was added to a beaker containing 50 mL of MB dye solution (50 mg/L) under continuous stirring at room temperature. The solution was stirred for 2 min to ensure the adsorption−desorption equilibrium of the dye on the composite. Then, 1 mL of fresh $NaBH_4$ solution (0.25 M) was rapidly injected into the mixture. Aliquots of samples were taken from the reaction mixture at predetermined time intervals. The MB dye solution's dark blue color quickly disappeared. The left-over MB dye solution concentration (residual MB dye solution concentration) was estimated by monitoring the time-dependent absorbance (in the range of 200−800 nm) with a UV−Vis spectrometer at 665 nm. In addition, two major factors that affect the reduction rate constants, including the mass of Ag-NPs/kaolin composite and concentration of MB dye solution, were investigated. Moreover, the degradation of MB with kaolin, Ag-NPs/kaolin composite-1, Ag-NPs/kaolin composite-2, Ag-NPs/kaolin composite-3, and Ag-NPs/kaolin composite-4 was investigated to examine the effect of silver nanoparticles loading on the surface of kaolin to its catalytic performance.

The catalytic reduction rate of MB dye solution, k_{red}, is estimated through pseudo-first-order kinetics fitting according to eq 1.[58]

$$\ln\left(\frac{C_t}{C_o}\right) = -k_{red}t \quad (1)$$

where C_t is the concentration of MB dye solution at equilibrium time t, C_o is the initial concentration of MB dye solution, and k_{red} is the reduction rate constant.

The percent removal efficiency of the catalyst was determined by eq 2.[59]

$$\%R_{MB} = \frac{C_o - C_t}{C_o} \times 100\% \quad (2)$$

C_o and C_t are the initial and equilibrium dye concentrations (mg/L).

2.5. Reusability Test. The successive catalytic activities of Ag-NPs/kaolin composite were explored to evaluate its reusability. For the first cycle, 10 mg of Ag-NPs/kaolin composite was added into the mixture of 15 mL of MB aqueous solution (100 mg/L) and 0.5 mL of $NaBH_4$ (0.25 M). The mixture was stirred for 10 min, and the Ag-NPs/kaolin composite was collected through 10 min centrifugation at 4000 rpm and reused for another five cycles in similar conditions.

3. RESULTS AND DISCUSSION

Raw kaolin was treated by a simple wet-beneficiation step. The beneficiated kaolin was used as a support material for the immobilization of Ag-NPs on its surface by using $NaBH_4$ as a reducing agent. Various physio-chemical techniques could confirm the immobilization of metal nanoparticles. The synthesized nanocatalyst was employed to efficiently reduce organic dye MB into leuco-MB.

3.1. Characteristics of Ag-NPs/Kaolin Composite. The UV−Vis spectroscopy technique is commonly used to understand metal nanoparticle formation by measuring the surface plasmon resonance (SPR) of metal electrons. The nanoparticle solution shows an absorption band in the UV−Vis wavelength range of 200−700 nm that is used to characterize the metal and metal oxide nanoparticles and gives information about the nanoparticle size, shape, stability, and aggregation.[60,61] For example, Ag-NPs exhibit a specific absorbance peak between 400 and 450 nm.[62]

Figure 1 depicts the UV−Vis spectra of beneficiated kaolin and fabricated Ag-NPs/kaolin composites. The absorption

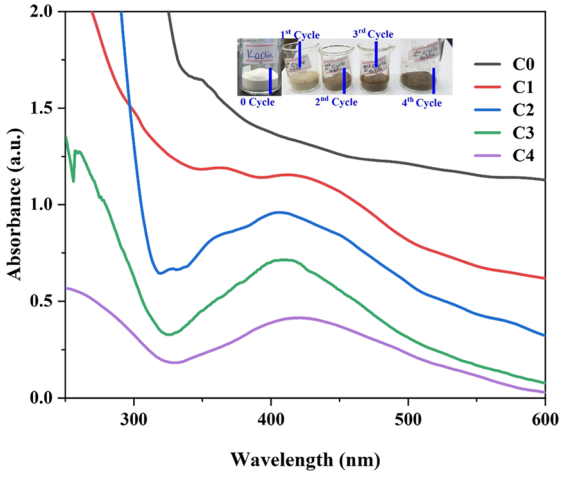

Figure 1. UV−vis absorption spectra of kaolin (C0), Ag-NPs/kaolin composite-1 (C1), Ag-NPs/kaolin composite-2 (C2), Ag-NPs/kaolin composite-3 (C3) and Ag-NPs/kaolin composite-4 (C4). Inset image shows the powder of beneficiated kaolin and composites in beakers.

peak at around 400 nm is attributed to the SPR of Ag-NPs, indicating the growth of Ag-NPs on the kaolin surface.[63−65] The SPR band arises due to the combined oscillations of nanoparticle conduction electrons in visible light. It is greatly influenced by the size and morphology of the nanoparticles.[66] The sharp band elucidates the formation of dispersed Ag-NPs

https://doi.org/10.1021/acsomega.2c05265
ACS Omega 2023, 8, 480−491

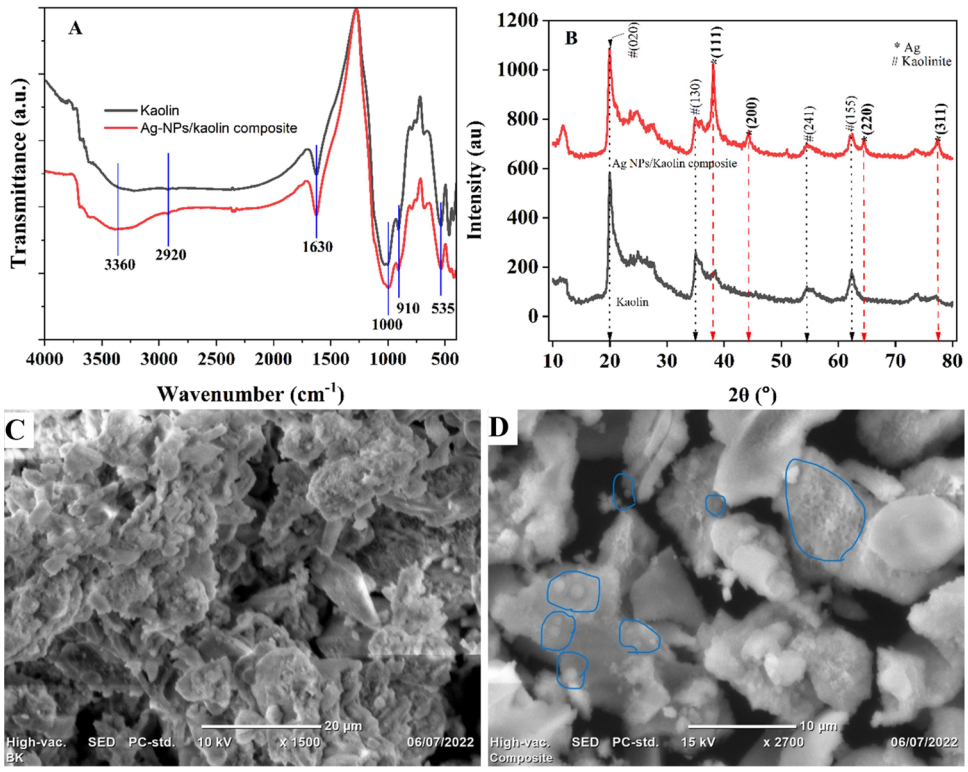

Figure 2. Characterizations of kaolin and Ag-NPs/kaolin composite including FT-IR spectra (A), XRD patterns (B), and SEM images of kaolin (C) and Ag-NPs/kaolin composite (D).

without forming aggregates or Ag_2O nanoparticles.[67] Furthermore, as the Ag-NP loading cycle increases, the peak maximum position shifts toward the higher wavelength, indicating that the Ag-NP size increases.[68] In addition, the color of the composite becomes darker with increasing cycle number, as shown in the inset image, confirming the Ag-NP size increase with successive cycles. Unlike impregnation of presynthesized Ag-NPs with kaolin or homogeneous precipitation of Ag-NPs in the mixture of Ag ions, kaolin, and reducing agents, the method grows Ag-NPs strongly coupled to kaolin surfaces.

The FT-IR spectra of beneficiated kaolin and Ag-NPs/kaolin composite are displayed in Figure 2A. The band 1630 cm^{-1} is attributed to water molecules absorbed on the beneficiated kaolin and Ag-NPs/kaolin composite surface.[69] The weak broadband peak around 3365 cm^{-1} represents hydroxyl stretching vibrations (Al-OH or Si-OH) and the characteristic band of kaolin.[56] Peaks around 1000 and 910 cm^{-1} correspond with silicon monoxide (Si−O) and Al−O stretching vibration related to quartz and disilicon oxide (Si−O−Si) symmetric stretch stretching vibration, respectively, indicating that silicon oxide is contained dominantly in the studied kaolin.[56] The small peak at 2350 cm^{-1} is attributed to the deformation of hydroxyl from the water molecule. The tiny weak peaks at 2920 cm^{-1} from the raw kaolin attribute aliphatic hydrocarbon (CH) stretching, indicating an organic impurity, but because of beneficiation, the presence is insignificant. The small peak at 790 cm^{-1} is attributed to metal impurity bonded with aluminum and hydroxyl (Al-Mg-OH) vibration.[56,70] A sharp and clear peak around 535 cm^{-1} corresponds with Si−O−Al bending vibration, indicating that aluminum oxide is also contained next to silicon oxide.[71,72]

The XRD patterns of Ag-NPs/kaolin composite are also shown in Figure 2B. According to previous studies, the diffraction peaks of kaolin found at 2θ = 19.94°, 35.30°, 38.48°, 54.52°, and 62.36° were ascribed to kaolinite. Compared with the XRD patterns of kaolin and Ag-NPs/kaolin composite, in the case of Ag-NPs/kaolin composite, several obvious diffraction peaks at 2θ = 38.04, 44.32, 64.48, and 77.48 that correspond to the reflections of (111), (200), (220), and (311) crystalline planes were observed, which is readily indexed to the face-centered-cubic (fcc) structure of the Ag crystal (JCPDS card No. 04-0783). Similar studies were reported.[22,23,40,73] The typical XRD peaks of Ag crystal revealed that the crystallized Ag-NPs could be successfully immobilized onto the kaolin surface.[22,73] Furthermore, the intensity ratio of (111) and (200) diffraction peaks is much higher than the typical values, indicating that Ag-NPs are oriented in the (111) plane.[74] Thus, the XRD pattern of the Ag-NPs/kaolin composite reveals that the Ag-NPs have an fcc geometry and are oriented in the (111) plane on the kaolin surface. The average crystalline particle size of the Ag-NPs grown on the kaolin surface was calculated using XRD data using the most intense 111 diffraction plane using the following Scherrer's formula (eq 3).[75]

$$D = \frac{k\lambda}{\beta\cos\theta} \tag{3}$$

where λ is the X-ray wavelength (0.15406 nm), β is the full width half maximum (FWHM) in radian, and θ is the peak angle. The average crystalline size of the Ag-NPs/kaolin composite was found to be 7.24 nm.

SEM analysis was used to determine the morphological feature of kaolin and Ag-NPs/kaolin composite. Figure 2D shows that the doping of Ag-NPs on the kaolin surface changes

https://doi.org/10.1021/acsomega.2c05265
ACS Omega 2023, 8, 480−491

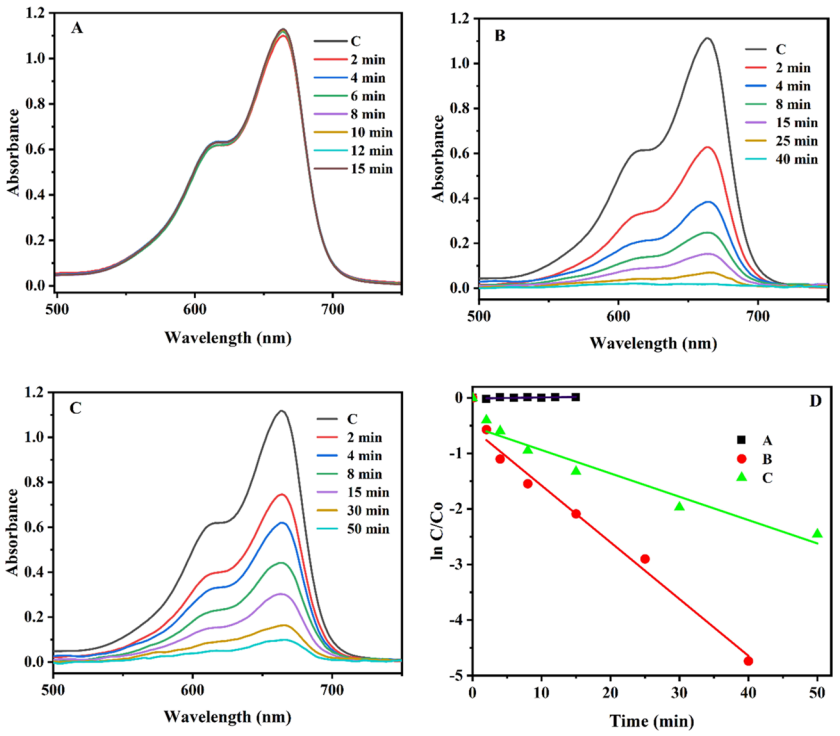

Figure 3. Successive UV−vis absorption spectra of MB dye aqueous solution (50 mL, 50 mg/L) within the presence of (A) $NaBH_4$ (0.25 M), (B) Ag-NPs/kaolin composite with $NaBH_4$ (0.25 M) and (C) Ag-NPs/kaolin composite. (D) Pseudo-first-order kinetics plots of (A−C).

its morphology and roughness compared to the pristine kaolin in Figure 2C. It confirms the successful deposition of Ag-NPs onto the surface of kaolin. More importantly, small bright particles are observed on the Ag-NPs/kaolin composite surface, indicating that Ag-NPs are uniformly distributed without agglomeration.[73] In general, all the above characterization results confirm that Ag-NPs can be loaded on the kaolin surfaces upon soaking in $AgNO_3$ solution and reducing using $NaBH_4$, which is a facile and efficient process to grow Ag-NPs directly on the kaolin surface.

The BET surface area, pore volume, and pore diameter were recorded by nitrogen adsorption−desorption measurement. For the Ag-NPs/kaolin composite, the BET surface area of 480.8 m^2/g was observed. The Ag-NPs/kaolin composite material has a porous structure, which was observed through the Barrett−Joyner−Halenda adsorption pore size distribution curve. A pore size diameter of 1.324 nm and a pore volume of 0.163 cm^3/g were observed. The observation indicates that the synthesized Ag-NPs/kaolin composite is highly porous.[27]

3.2. Catalytic Test. *3.2.1. Catalytic Degradation of MB Dye.* The catalytic activity of the synthesized Ag-NPs/kaolin composite was investigated using the degradation reaction of MB dye in the presence of $NaBH_4$. MB dye is a cationic thiazine dye that finds many uses in many fields, including chemistry and biology.[76] The aqueous solution of the oxidized form of MB is deep blue in color, and its reduced form (leuco form) is colorless. The UV−vis absorption spectrum of an aqueous solution of MB shows peaks at 290 and 664 nm with a hump at 612 nm due to $\pi \rightarrow \pi^*$ and $n \rightarrow \pi^*$ transitions, respectively.[77] The reduction of MB into its colorless form can be followed spectrophotometrically by monitoring the absorption maximum at 664 nm.

Even though sodium borohydride is a strong reducing agent, the aqueous solution of $NaBH_4$ is unable to effectively reduce MB due to the appreciable difference in redox potentials of this dye and $NaBH_4$.[78] In this study, the degradation of MB by $NaBH_4$ was performed in the presence and absence of the Ag-NPs/kaolin composite. The blank experiments conducted on the degradation of MB by $NaBH_4$ without adding the composite material showed no change in color as well as the intensity of λ_{max} at 664 nm (Figure 3A). This shows that it is not degraded by $NaBH_4$ alone or the degradation of it in the absence of composite material occurs at a negligibly slow rate which is difficult to identify. However, the rate of degradation was greatly enhanced upon the addition of the catalyst, indicating the immense catalytic effect of the synthesized Ag-NPs/kaolin composite in this reaction (Figure 3B). This was evident from the fading and ultimate disappearance of the deep blue color of MB and the rapid decrease in the intensity of λ_{max} at 664 nm to approximately zero in 40 min, indicating the complete degradation of MB solution. Figure 3C also shows the addition of Ag-NPs/kaolin composite into the MB dye solution in the absence of $NaBH_4$, with which a decrease in the spectra of MB has been observed but does not completely disappear until 50 min reaction time. The decrease in spectra may be due to the adsorption of MB dye on the composite catalyst due to kaolinite.[79] Furthermore, the kinetics of the MB reduction was also investigated to determine the reduction rate constant, k_{red}, (Figure 3D). The catalytic rate of MB fitted by pseudo-first-order reaction kinetics was applied to evaluate the catalytic activity. Moreover, good linear correlation coefficient values of the plot of ln C/C_o versus reaction time can be observed in Table 1, indicating that the reactions could be well described by pseudo-first-order kinetics.

Furthermore, the loading content of Ag-NPs could influence the catalytic activity on dye degradation. To increase the Ag-NPs loading content on the kaolin surface, the synthesis procedure was done repeatedly to obtain different cycles. The

https://doi.org/10.1021/acsomega.2c05265
ACS Omega 2023, 8, 480−491

Table 1. Kinetic Parameters of the Catalyst with Different Conditions to $NaBH_4$

mass of the catalyst	MB dye solution	$NaBH_4$ solution	rate constant	correlation coefficient
0		0.25 M, 1 mL	0.00177 min^{-1}	0.34532
5 mg	50 mg/L, 50 mL	0.25 M, 1 mL	0.1022 min^{-1}	0.98461
5 mg		0	0.04203 min^{-1}	0.94055

obtained materials in particular Ag-NPs/kaolin composite-1, Ag-NPs/kaolin composite-2, Ag-NPs/kaolin composite-3, and Ag-NPs/kaolin composite-4 were tested to select the best cycle toward the catalytic reduction of MB dye in the presence of $NaBH_4$ as a reducing agent. Figure 4 demonstrates the successive UV−vis spectra of the catalytic reduction of MB dye using the four fabricated materials in addition to bare kaolin. The degradation of MB was much easier with Ag-NPs/kaolin composite-3 (Figure 4D) and Ag-NPs/kaolin composite-4 (Figure 4E) than that of Ag-NPs/kaolin composite-1 (Figure 4B) and Ag-NPs/kaolin composite-2 (Figure 4C), owing to the higher content of Ag-NPs on the kaolin surface. The absorbance peak at 664 nm almost disappeared within a few minutes in the presence of Ag-NPs/kaolin composite-3. Furthermore, the increase of the reduction rate constant, k_{red}, from kaolin to Ag-NPs/Kaolin composite-4 (0.18766, 0.22052, 0.31147, 0.75327, and 0.78216 min^{-1}, respectively) confirms that Ag-NPs/kaolin composite-3 and 4 have the best catalytic efficiencies for the reduction of MB dye solution which is fitted by pseudo-first-order kinetics (Figure 4F). The removal efficiency of Ag-NPs/kaolin composite-3 (10 mg) in the presence of $NaBH_4$ (0.25 M) for 50 mL (50 mg L^{-1}) MB within 2 min reaction time is 96.32%, whereas that for Ag-NPs/kaolin composite-4 is 97.05% with the same conditions. Therefore, choosing the best loading content of Ag-NPs

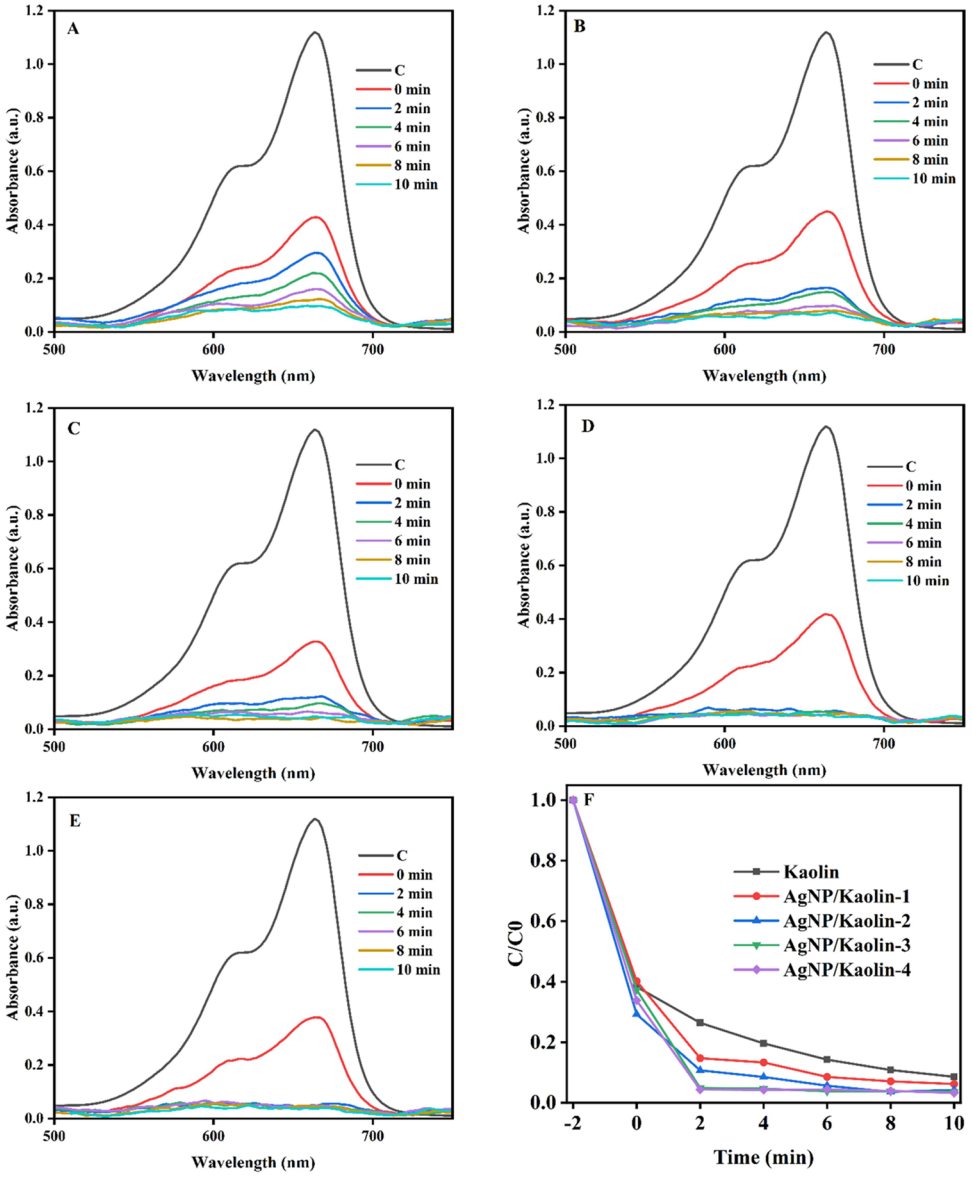

Figure 4. Successive UV−vis absorption spectra of MB dye aqueous solution (50 mL, 50 mg/L) with the presence of $NaBH_4$ (0.25 M) and 10 mg of (A) kaolin, (B) Ag-NPs/kaolin composite-1, (C) Ag-NPs/kaolin composite-2, (D) Ag-NPs/kaolin composite-3, (E) Ag-NPs/kaolin composite-4, and (F) absorption rate curves of the catalytic reduction of MB dye solution with different composites and precursor kaolin.

https://doi.org/10.1021/acsomega.2c05265
ACS Omega 2023, 8, 480−491

through the cycles is crucial. Since Ag-NPs/kaolin composite-3 exhibited a satisfactory catalytic performance on MB dye reduction, it was selected as the catalyst for the following experiments.

Theoretically, the catalytic reaction involves the adsorption of dye molecules and BH_4^- ions onto the catalyst surface, and the electron transfer from the donor BH_4^- to the acceptor dye molecules, which has been collectively demonstrated in previous studies.[22,50,80] Herein, the electrons donated by BH_4^- will transfer to the electron relay of Ag-NPs; then, MB molecules can capture them from Ag-NPs, thereby resulting in the redox reduction of MB and generating its reduced form (leuco-MB) (Scheme 2).[80,81] This gives concrete evidence for

Scheme 2. Proposed Reduction Mechanism of MB Dye by the Ag-NPs/Kaolin Composite in the Presence of $NaBH_4$

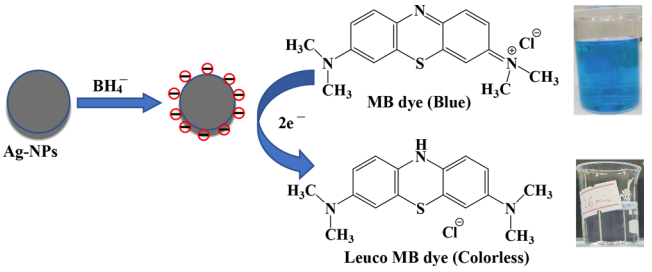

the involvement of nanoparticles as electron relay systems during the redox process. Therefore, the presence of Ag-NPs could enhance the degradation of the MB dye.

3.2.2. Effect of MB Dye Concentration on the Catalytic Activity of the Ag-NPs/Kaolin Composite. To evaluate the catalytic activity of Ag-NPs/Kaolin composite toward MB aqueous solution degradation with different concentrations, three different concentrations (30, 40, and 50 mg/L) of MB solution were used for the tests. As shown in Figure 5, the degradation time increased with MB concentration. The intensity of the maximum absorption peak dropped sharply within 12, 20, and 40 min after adding the catalyst into the corresponding MB solution with a concentration of 30, 40, and 50 mg/L, respectively. Furthermore, the complete degradation of higher dye solution concentrations required more time under the same conditions. The increase in dye concentration would lead to the increased competition of electron capture among dye molecules, whereas the catalytic capacity was finite at a fixed mass of catalyst; thus, the dye reduction decreased at a higher dye concentration. Moreover, Figure 5D illustrates the pseudo-first-order linear fitting of the different MB dye solution concentrations used to calculate the reduction rate constants, k_{red} (Table 2). The reduction rate constants

Table 2. Catalytic Removal Efficiency of Composite with Different MB Dye Solution Concentrations

catalyst mass	MB solution (50 mL)	rate constant (min^{-1})	correlation coefficient	%R	time (min)
5 mg	30 mg/L	0.34854	0.99359	98.61	12
	40 mg/L	0.26403	0.99023	98.28	15
	50 mg/L	0.0872	0.97827	97.71	40

decrease from 0.35 to 0.087 min^{-1} as the MB dye solution concentration increases from 30 to 50 mg/L when the mass of Ag-NPs/kaolin composite and concentration of $NaBH_4$ are fixed at 5 mg and 0.25 M, respectively (Table 2).

3.2.3. Effect of Catalyst Dosage on the Catalytic Activity of Ag-NPs/Kaolin Composite. To evaluate the catalytic activity of the Ag-NPs/kaolin composite toward MB dye aqueous solution with different amounts of catalysts, three

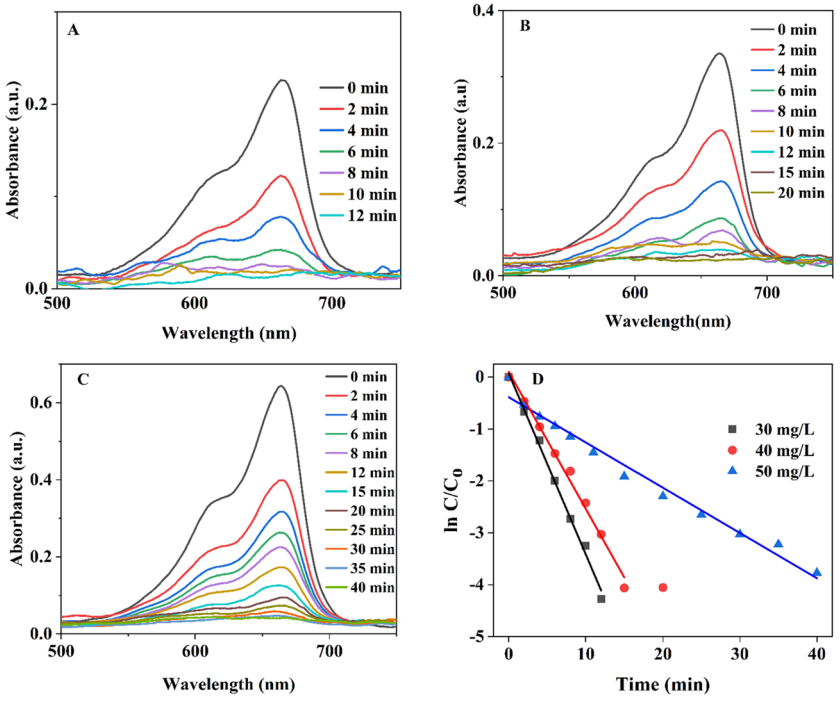

Figure 5. Successive UV−vis absorption spectra of different concentrations of MB dye aqueous solution (50 mL) with (A) 30 mg/L, (B) 40 mg/L, and (C) 50 mg/L, in the presence of $NaBH_4$ (0.25 M) and Ag-NPs/kaolin composite (5 mg). (D) First-order kinetics plots of catalytic reduction of MB dye solution with different concentrations.

https://doi.org/10.1021/acsomega.2c05265
ACS Omega 2023, 8, 480−491

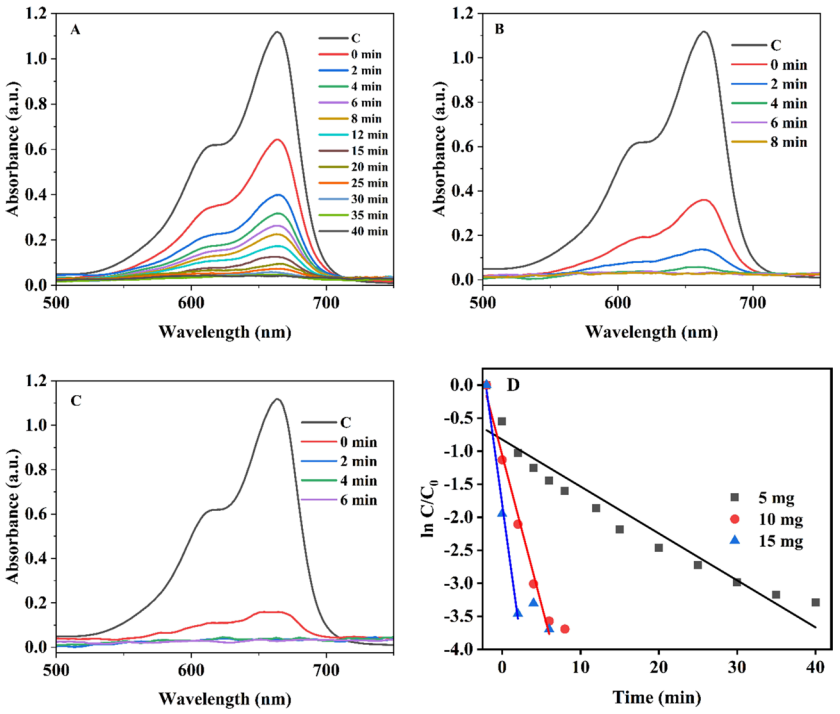

Figure 6. Successive UV−vis absorption spectra of MB aqueous solution (50 mL, 50 mg/L) with different catalyst dosages, (A) 5 mg, (B) 10 mg, and (C) 15 mg, in the presence of $NaBH_4$ (0.25 M) and (D) pseudo-first-order kinetics plots of catalytic reduction of MB dye solution with different catalyst dosages.

different masses (5, 10, and 15 mg) of the composite amount were used. As shown in Figure 6, the catalytic reduction of MB was faster in the reaction system with a higher catalyst dosage. The intensity of the maximum absorption peak dropped sharply within 2, 6, and 10 min after adding 5, 10, and 15 mg of catalyst into the corresponding MB solution (50 mg/L). Furthermore, the complete degradation of dye within a short time required a high amount of Ag-NPs/kaolin composite, and it needed more time at the small amount of the Ag-NPs/kaolin composite. The increased amount of the catalyst would lead to the increased electron relay, whereas the MB capacity was finite at a fixed concentration; thus, the dye reduction rate decreased at a small amount of catalyst. The reduction rate constants (k_{red}) were calculated for each catalyst dosage treatment of MB dye solution from the pseudo-first-order kinetic plot, as shown in Figure 6D (Table 3). The reaction

Table 3. Catalytic Removal Efficiency of Composite with Different Dosages

catalyst mass	MB solution (50 mL)	rate constant (min^{-1})	correlation coefficient	%R	time (min)
5 mg		0.07107	0.91441	96.27	40
10 mg	50 mg/L	0.45094	0.98226	97.51	8
15 mg		0.86523	0.98951	97.52	4

rate increased with the increase of catalyst dosage due to the increased electron transferability with good linear correlation coefficient values. Thus, an appropriate catalyst dosage used for the dye reduction is necessary to make the response more effective. By comparing the catalytic reduction of MB using other different nanocatalysts, we concluded that this as-prepared Ag-NPs/kaolin composite showed a satisfactory catalytic performance on dye reduction. To evaluate the MB dye reduction efficiency more broadly, the data obtained from the reduction of the MB dye in the presence of $NaBH_4$ on the Ag-NPs/kaolin composite were compared with some of the studies given in Table 4.

3.3. Reusability of the Composite. The recyclability and stability of the composite are the critical properties to reduce the cost and maintain their persistent and efficient catalytic performances for their practical applications in wastewater treatment. Kaolin was used to support Ag-NPs to achieve a low cost and a simple recovery since it is a cheap natural resource with easy sedimentation in aqueous dispersion. The successive four catalytic cycles of the Ag-NPs/kaolin composite were tested to determine its recyclability and catalytic performances on the reduction of MB dye solution. Figure 7 shows that Ag-NPs/kaolin composite has excellent catalytic performances achieving above 97% reduction efficiency in the tested five-time cycles. The kaolin plays an essential role in stabilizing Ag-NPs and preventing their aggregation during the repeated catalytic reduction of the enormous amount of MB dye solution. The excellent stability and reusability indicated that the Ag-NPs/kaolin composite might have a good application in MB dye wastewater treatment.

4. CONCLUSIONS

In conclusion, a facile and cost-effective synthesis method is developed successfully by in situ growth of Ag-NPs on the locally available and inexpensive kaolin surface through the chemical reduction of silver ions by $NaBH_4$. The prepared Ag-NPs/kaolin composite exhibits excellent catalytic performances to reduce a model organic dye MB in the presence of $NaBH_4$ and to remove its color through the fast removal rate of MB dye from aqueous solutions. The remarkable catalytic reduction property is attributed to the high loading amount of well-dispersed Ag-NPs on the kaolin surface. The Ag-NPs/kaolin composite (15 mg) degraded 97.5% of 50 mL of MB

https://doi.org/10.1021/acsomega.2c05265
ACS Omega 2023, 8, 480−491

Table 4. Comparison of the Catalytic Activity of Ag-NPs/Kaolin Composite with Some Catalysts Reported in the Literature for the Reduction of MB Dye

catalysts	dosage	MB dye concentration	time (min)	reduction efficiency (%)	references
$AgFe_2O_4$/MWCNT nanoparticle	12 mg	24 mg/L	75	98.5	82
Ag NPs@Mt	800 mg/L	100 mg/L (1 mL)		98	73
Sb-doped $Mo(O,S)_3$ oxy-sulfide nanoplate	20 mg	10 mg/L (100 mL)	60	99.7	83
Ag-K-T composite	0.5 g/L	1.6 mg/L	70	~100	26
Fe2O3-graphene-Ag composite	1 g/L	5 mg/L (100 mL)	90	83	84
Ag/Fe3O4@GO	10 mg	16 mg/L (50 mL)	10	98	9
Ag-NPs/kaolin composite	15 mg	50 mg/L (50 mL)	4	97.5	this work

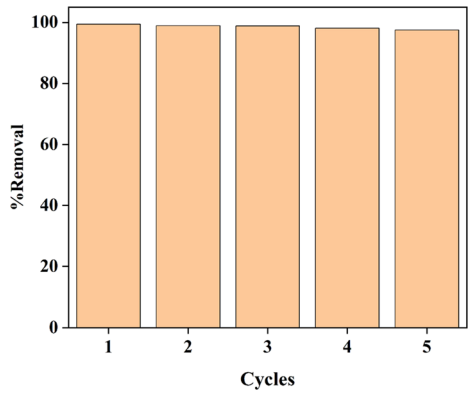

Figure 7. Recycling of the Ag-NPs/kaolin composite for the degradation of MB dye solution with $NaBH_4$.

dye solution of 50 mg/L within 4 min in the presence of $NaBH_4$ with a rate constant of 0.865 min^{-1}. Ag-NP catalytic activity encourages the Ag-NPs/kaolin composite system to achieve superior MB dye catalytic reduction efficiency. This easy synthesis method may apply to other nanoparticles on diverse support material surfaces. It may pave a new way to synthesize the low-cost, high-performance catalyst on a large scale with significant potential applications in wastewater treatment. The prepared catalyst showed excellent activity and could be reused in multiple catalytic cycles with very little loss in its activity.

AUTHOR INFORMATION

Corresponding Authors

Belete Asefa Aragaw − *Department of Chemistry, College of Science, Bahir Dar University, Bahir Dar 6000, Ethiopia;* orcid.org/0000-0003-4801-7197; Email: beliyeeed@gmail.com

Minaleshewa Atlabachew − *Department of Chemistry, College of Science, Bahir Dar University, Bahir Dar 6000, Ethiopia;* orcid.org/0000-0003-3261-8326; Email: atminale2004@yahoo.com

Authors

Zinabu Gashaw Asmare − *Department of Chemistry, College of Science, Bahir Dar University, Bahir Dar 6000, Ethiopia;* Present Address: Department of Chemistry, College of Natural and Computational Sciences, Debre Tabor University, P.O. Box 272, Debre Tabor 6300, Ethiopia

Tessera Alemneh Wubieneh − *Department of Materials Science and Engineering, College of Science, Bahir Dar University, Bahir Dar 6000, Ethiopia*

Complete contact information is available at: https://pubs.acs.org/10.1021/acsomega.2c05265

Notes

The authors declare no competing financial interest.

ACKNOWLEDGMENTS

Mr. Zinabu Gashaw Asmare is thankful to Debre Tabor University for sponsoring his PhD study. The authors are thankful to the college of science of Bahir Dar University for the laboratory facilities pertaining to this study. This study was financially supported by the mega project funds of the College of Science, Bahir Dar University.

REFERENCES

(1) Patel, H.; Shakhreliya, S.; Maurya, R.; Pandey, V. C.; Gohil, N.; Bhattacharjee, G.; Alzahrani, K. J.; Singh, V.CRISPR-assisted strategies for futuristic phytoremediation. In *Assisted Phytoremediation*; Pandey, V., Ed.; Elsevier, 2022; pp 203−220.

(2) Tang, X.; Zeng, G.; Fan, C.; Zhou, M.; Tang, L.; Zhu, J.; Wan, J.; Huang, D.; Chen, M.; Xu, P.; Zhang, C.; Lu, Y.; Xiong, W. Chromosomal expression of CadR on Pseudomonas aeruginosa for the removal of Cd (II) from aqueous solutions. *Sci. Total Environ.* **2018**, *636*, 1355−1361.

(3) Wang, Y.; Zhu, Y.; Hu, Y.; Zeng, G.; Zhang, Y.; Zhang, C.; Feng, C. How to construct DNA hydrogels for environmental applications: advanced water treatment and environmental analysis. *Small* **2018**, *14*, No. 1703305.

(4) Xiong, W.; Zeng, Z.; Li, X.; Zeng, G.; Xiao, R.; Yang, Z.; Zhou, Y.; Zhang, C.; Cheng, M.; Hu, L.; Zhou, C.; Qin, L.; Xu, R.; Zhang, Y. Multi-walled carbon nanotube/amino-functionalized MIL-53 (Fe) composites: remarkable adsorptive removal of antibiotics from aqueous solutions. *Chemosphere* **2018**, *210*, 1061−1069.

(5) Yang, Y.; Zeng, Z.; Zhang, C.; Huang, D.; Zeng, G.; Xiao, R.; Lai, C.; Zhou, C.; Guo, H.; Xue, W.; Cheng, M.; Wang, W.; Wang, J. Construction of iodine vacancy-rich BiOI/Ag@ AgI Z-scheme heterojunction photocatalysts for visible-light-driven tetracycline degradation: transformation pathways and mechanism insight. *Chem. Eng. J.* **2018**, *349*, 808−821.

(6) Yi, H.; Huang, D.; Qin, L.; Zeng, G.; Lai, C.; Cheng, M.; Ye, S.; Song, B.; Ren, X.; Guo, X. Selective prepared carbon nanomaterials for advanced photocatalytic application in environmental pollutant treatment and hydrogen production. *Appl. Catal., B* **2018**, *239*, 408−424.

(7) Zhou, C.; Lai, C.; Zhang, C.; Zeng, G.; Huang, D.; Cheng, M.; Hu, L.; Xiong, W.; Chen, M.; Wang, J.; Yang, Y.; Jiang, L. Semiconductor/boron nitride composites: synthesis, properties, and photocatalysis applications. *Appl. Catal., B* **2018**, *238*, 6−18.

(8) Luu, T. V. H.; Luu, M. D.; Dao, N. N.; Le, V. T.; Nguyen, H. T.; Doan, V. D. Immobilization of C/Ce-codoped ZnO nanoparticles on multi-walled carbon nanotubes for enhancing their photocatalytic activity. *J. Dispersion Sci. Technol.* **2021**, *42*, 1311−1322.

(9) Doan, V.-D.; Nguyen, N.-V.; Nguyen, T. L.-H.; Tran, V. A.; Le, V. T. High-efficient reduction of methylene blue and 4-nitrophenol by silver nanoparticles embedded in magnetic graphene oxide. *Environ. Sci. Pollut. Res.* **2021**, DOI: 10.1007/s11356-021-13597-z.

(10) Hassaan, M.; El Nemr, A. Health and Environmental Impacts of Dyes: Mini Review. *Am. J. Environ. Sci. Eng.* **2017**, *1*, 64−67.

(11) Dao, M. U.; Le, H. S.; Hoang, H. Y.; Tran, V. A.; Doan, V. D.; Le, T. T. N.; Sirotkin, A.; Le, V. T. Natural core-shell structure activated carbon beads derived from Litsea glutinosa seeds for removal of methylene blue: Facile preparation, characterization, and adsorption properties. *Environ. Res.* **2021**, *198*, No. 110481.
(12) Holkar, C. R.; Jadhav, A. J.; Pinjari, D. V.; Mahamuni, N. M.; Pandit, A. B. A critical review on textile wastewater treatments: Possible approaches. *J. Environ. Manage.* **2016**, *182*, 351−366.
(13) Saha, J.; Begum, A.; Mukherjee, A.; Kumar, S. A novel green synthesis of silver nanoparticles and their catalytic action in reduction of Methylene Blue dye. *Sustainable Environ. Res.* **2017**, *27*, 245−250.
(14) Stewart, S.; Wei, Q.; Sun, Y. Surface chemistry of quantum-sized metal nanoparticles under light illumination. *Chem. Sci.* **2021**, *12*, 1227−1239.
(15) Sheerazi, Z.; Ahmed, M.Nano-Adsorbents and Nano-Catalysts for Wastewater Treatment. In *Emerging Nanomaterials for Advanced Technologies*; Springer, 2022; pp 517−539.
(16) Sharma, K.; Ali, M.; Singh, R.; Majhi, S.; Sharma, S.; Tripathi, C. S. P.; Guin, D. Silver nanoparticles decorated on graphene oxide modified polyester fabric: Catalytic reduction of 4-nitrophenol, organic dyes and SERS application. *J. Phys. Chem. Solids* **2022**, *165*, No. 110640.
(17) Liu, Y.; Zhou, H.; Wang, J.; Li, S.; Li, Z.; Zhang, J. Core-shell Fe3O4@catechol-formaldehyde trapped satellite-like silver nanoparticles toward catalytic reduction in cationic and anionic dyes. *Vacuum* **2022**, *202*, No. 111204.
(18) Naveas, N.; Manso-Silván, M.; Carmona, E.; Garrido, K.; Hernández-Montelongo, J.; Recio-Sánchez, G. Green synthesized silver nanoparticles decorated on nanostructured porous silicon as an efficient platform for the removal of organic dye methylene blue. *Green Chem. Lett. Rev.* **2022**, *15*, 108−115.
(19) Alahdal, F. A. M.; Qashqoosh, M. T. A.; Kadaf Manea, Y.; Salem, M. A. S.; Hasan Khan, R.; Naqvi, S. Ultrafast fluorescent detection of hexavalent chromium ions, catalytic efficacy and antioxidant activity of green synthesized silver nanoparticles using leaf extract of P. austroarabica. *Environ. Nanotechnol., Monit. Manage* **2022**, *17*, No. 100665.
(20) Cai, L.; Zhang, L.; Xu, X. One-step synthesis of ultra-small silver nanoparticles-loaded triple-helix β-glucan nanocomposite for highly catalytic hydrogenation of 4-nitrophenol and dyes. *Chem. Eng. J.* **2022**, *442*, No. 136114.
(21) Khan, S. A.; Jain, M.; Pandey, A.; Pant, K. K.; Ziora, Z. M.; Blaskovich, M. A. T.; Shetti, N. P.; Aminabhavi, T. M. Leveraging the potential of silver nanoparticles-based materials towards sustainable water treatment. *J. Environ. Manage.* **2022**, *319*, No. 115675.
(22) He, K.; Yan, M.; Huang, Z.; Zeng, G.; Chen, A.; Huang, T.; Li, H.; Ren, X.; Chen, G. Fabrication of ploydopamine−kaolin supported Ag nanoparticles as effective catalyst for rapid dye decoloration. *Chemosphere* **2019**, *219*, 400−408.
(23) Somasundaram, C. K.; Atchudan, R.; Edison, T. N. J. I.; Perumal, S.; Vinodh, R.; Sundramoorthy, A. K.; Babu, R. S.; Alagan, M.; Lee, Y. R. Sustainable Synthesis of Silver Nanoparticles Using Marine Algae for Catalytic Degradation of Methylene Blue. *Catalysts* **2021**, *11*, 1377.
(24) Yin, Y.; Shen, M.; Tan, Z.; Yu, S.; Liu, J.; Jiang, G. Particle coating-dependent interaction of molecular weight fractionated natural organic matter: impacts on the aggregation of silver nanoparticles. *Environ. Sci. Technol.* **2015**, *49*, 6581−6589.
(25) Hernández, D.; Vidal, J. C.; Laborda, F.; Pérez-Arantegui, J.; Giménez-Ingalaturre, A. C.; Castillo, J. R. Detection, size characterization and quantification of silver nanoparticles in consumer products by particle collision coulometry. *Microchim. Acta* **2021**, *188*, 1−10.
(26) Sharma, S.; Devi, A.; Bhattacharyya, K. G. Photocatalytic Degradation of Methylene Blue in Aqueous Solution with Silver-Kaolinite-Titania Nanocomposite under Visible Light Irradiation. *J. Nanostruct.* **2022**, *12*, 426−445.
(27) Kumar, Y.; Rani, S.; Shabir, J.; Kumar, L. S. Nitrogen-Rich and Porous Graphitic Carbon Nitride Nanosheet-Immobilized Palladium Nanoparticles as Highly Active and Recyclable Catalysts for the Reduction of Nitro Compounds and Degradation of Organic Dyes. *ACS Omega* **2020**, *5*, 13250−13258.
(28) Fatimah, I.; Fadillah, G.; Yanti, I.; Doong, R.-a. Clay-Supported Metal Oxide Nanoparticles in Catalytic Advanced Oxidation Processes: A Review. *Nanomaterials* **2022**, *12*, 825.
(29) Mundkur, N.; Khan, A. S.; Khamis, M. I.; Ibrahim, T. H.; Nancarrow, P. Synthesis and characterization of clay-based adsorbents modified with alginate, surfactants, and nanoparticles for Methylene blue removal. *Environ. Nanotechnol., Monit. Manage* **2022**, *17*, No. 100644.
(30) Yilmaz, A. K.; Hilal Gubbuk, I. Synthesis and Characterization of Ag/Montmorillonite Clay Nanocomposite for Chemical Catalytic Degradation of Azo Pollutants. *Russ. J. Phys. Chem. A* **2022**, *96*, 842−848.
(31) Tharmaraj, V.; Anbu Anjugam Vandarkuzhali, S.; Karthikeyan, G.; Pachamuthu, M. Efficient and recyclable AuNPs/aminoclay nanocomposite catalyst for the reduction of organic dyes. *Surf. Interfaces* **2022**, *32*, No. 102052.
(32) Asli, B.; Abdelkrim, S.; Zahraoui, M.; Mokhtar, A.; Hachemaoui, M.; Bennabi, F.; Ahmed, A. B.; Sardi, A.; Boukoussa, B. Catalytic Reduction and Antibacterial Activity of MCM-41 Modified by Silver Nanoparticles. *Silicon* **2022**, DOI: 10.1007/s12633-022-01963-6.
(33) Shanmugaraj, K.; Campos, C. H.; Mangalaraja, R. V.; Nandhini, K.; Aepuru, R.; Torres, C. C.; Singh, D. P.; Kumar, D.; Ilanchelian, M.; Sharma, A.; et al. Gold nanoparticle−decorated earth-abundant clay nanotubes as catalyst for the degradation of phenothiazine dyes and reduction of 4-(4-nitrophenyl)morpholine. *Environ. Sci. Pollut. Res.* **2022**, DOI: 10.1007/s11356-022-19523-1.
(34) Sajid, M. Bentonite-modified electrochemical sensors: a brief overview of features and applications. *Ionics* **2018**, *24*, 19−32.
(35) Padil, V. V. T.; Akshay Kumar, K. P.; Murugesan, S.; Torres-Mendieta, R.; Wacławek, S.; Cheong, J. Y.; Černík, M.; Varma, R. S. Sustainable and safer nanoclay composites for multifaceted applications. *Green Chem.* **2022**, *24*, 3081−3114.
(36) Yadav, D. K.; Gupta, R.; Ganesan, V.; Sonkar, P. K.; Rastogi, P. K. Electrochemical sensing platform for hydrogen peroxide determination at low reduction potential using silver nanoparticle-incorporated bentonite clay. *J. Appl. Electrochem.* **2016**, *46*, 103−112.
(37) Luon, N. T.; Long, N. Q.Catalytic oxidation of formaldehyde over silver supported on ZSM-5: The role of Ag and mesopores. In *IOP Conference Series: Earth and Environmental Science*; IOP Publishing, vol *964*, 2022; p 012026.
(38) Zou, Y.; Hu, Y.; Shen, Z.; Yao, L.; Tang, D.; Zhang, S.; Wang, S.; Hu, B.; Zhao, G.; Wang, X. Application of aluminosilicate clay mineral-based composites in photocatalysis. *J. Environ. Sci.* **2022**, *115*, 190−214.
(39) Zyoud, A. H.; Zubi, A.; Zyoud, S. H.; Hilal, M. H.; Zyoud, S.; Qamhieh, N.; Hajamohideen, A.; Hilal, H. S. Kaolin-supported ZnO nanoparticle catalysts in self-sensitized tetracycline photodegradation: zero-point charge and pH effects. *Appl. Clay Sci.* **2019**, *182*, No. 105294.
(40) Dou, Y.; Tu, F.; Wu, Y.; Wang, X.; Lu, G.; Zhao, L. Facile preparation of Kaolin supported silver nanoparticles mediated by Thymbra spicata extract and investigation of the anti-human lung cancer properties. *J. Saudi Chem. Soc.* **2021**, *25*, No. 101303.
(41) Mustapha, S.; Tijani, J.; Egbosiuba, T.; Sumaila, A.; Amigun, T.; Salihu, A.; Ibrahim, Y.; Ndamitso, M.; Abdulkareem, S.Sol−gel Synthesis of Kaolin/TiO2 Nanocomposites for Photocatalytic Degradation of Tannery Wastewater. In *Industrial Wastewater Treatment*; Springer, 2022; pp 323−343.
(42) Wang, H.; Li, C.; Peng, Z.; Zhang, S. Characterization and thermal behavior of kaolin. *J. Therm. Anal. Calorim.* **2011**, *105*, 157−160.
(43) Kanakaraju, D.; Anak Kutiang, F. D.; Lim, Y. C.; Goh, P. S. Recent progress of Ag/TiO2 photocatalyst for wastewater treatment: Doping, co-doping, and green materials functionalization. *Appl. Mater. Today* **2022**, *27*, No. 101500.

https://doi.org/10.1021/acsomega.2c05265
ACS Omega 2023, 8, 480−491

(44) Tunega, D.; Zaoui, A. Mechanical and bonding behaviors behind the bending mechanism of kaolinite clay layers. *J. Phys. Chem. C* **2020**, *124*, 7432−7440.
(45) Yariv, S. The effect of tetrahedral substitution of Si by Al on the surface acidity of the oxygen plane of clay minerals. *Int. Rev. Phys. Chem.* **1992**, *11*, 345−375.
(46) Unuabonah, E. I.; Adewuyi, A.; Kolawole, M. O.; Omorogie, M. O.; Olatunde, O. C.; Fayemi, S. O.; Günter, C.; Okoli, C. P.; Agunbiade, F. O.; Taubert, A. Disinfection of water with new chitosan-modified hybrid clay composite adsorbent. *Heliyon* **2017**, *3*, No. e00379.
(47) Yiga, V. A.; Lubwama, M.; Olupot, P. W. Thermal and alkali modification of kaolin for potential utilization as filler material in fiber-reinforced polylactic acid composites. *J. Therm. Anal. Calorim.* **2022**, *147*, 11077−11091.
(48) David, M. K.; Okoro, U. C.; Akpomie, K. G.; Okey, C.; Oluwasola, H. O. Thermal and hydrothermal alkaline modification of kaolin for the adsorptive removal of lead (II) ions from aqueous solution. *SN Appl. Sci.* **2020**, *2*, 1134.
(49) Seku, K.; Kishore Kumar, K.; Narasimha, G.; Bhagavanth Reddy, G.Chapter 7 - Bio-mediated synthesis of silver nanoparticles via microwave-assisted technique and their biological applications. In *Green Synthesis of Silver Nanomaterials*; Abd-Elsalam, K. A., Ed.; Elsevier, 2022; pp 149−188.
(50) Joseph, S.; Mathew, B. Microwave-assisted green synthesis of silver nanoparticles and the study on catalytic activity in the degradation of dyes. *J. Mol. Liq.* **2015**, *204*, 184−191.
(51) He, K.; Zeng, Z.; Chen, A.; Zeng, G.; Xiao, R.; Xu, P.; Huang, Z.; Shi, J.; Hu, L.; Chen, G. Advancement of Ag−graphene based nanocomposites: an overview of synthesis and its applications. *Small* **2018**, *14*, No. 1800871.
(52) Huang, Z.; He, K.; Song, Z.; Zeng, G.; Chen, A.; Yuan, L.; Li, H.; Hu, L.; Guo, Z.; Chen, G. Antioxidative response of Phanerochaete chrysosporium against silver nanoparticle-induced toxicity and its potential mechanism. *Chemosphere* **2018**, *211*, 573−583.
(53) Zhang, L.; Zhang, J.; Zeng, G.; Dong, H.; Chen, Y.; Huang, C.; Zhu, Y.; Xu, R.; Cheng, Y.; Hou, K.; Cao, W.; Fang, W. Multivariate relationships between microbial communities and environmental variables during co-composting of sewage sludge and agricultural waste in the presence of PVP-AgNPs. *Bioresour. Technol.* **2018**, *261*, 10−18.
(54) Song, K. C.; Lee, S. M.; Park, T. S.; Lee, B. S. Preparation of colloidal silver nanoparticles by chemical reduction method. *Korean J. Chem. Eng.* **2009**, *26*, 153−155.
(55) Chandrasekhar, S.; Ramaswamy, S. Influence of mineral impurities on the properties of kaolin and its thermally treated products. *Appl. Clay Sci.* **2002**, *21*, 133−142.
(56) Aragaw, T. A.; Angerasa, F. T. Synthesis and characterization of Ethiopian kaolin for the removal of basic yellow (BY 28) dye from aqueous solution as a potential adsorbent. *Heliyon* **2020**, *6*, No. e04975.
(57) Salahudeen, N.; Ahmed, A. S. Effect of Beneficiation on the Characteristics of Gambe and Pindiga Bentonitic Clays. *J. Mod. Chem. Chem. Technol.* **2016**, *7*, 20−26.
(58) Du, S.; Liao, Z.; Qin, Z.; Zuo, F.; Li, X. Polydopamine microparticles as redox mediators for catalytic reduction of methylene blue and rhodamine B. *Catal. Commun.* **2015**, *72*, 86−90.
(59) Momeni, M.; Ghayeb, Y.; Menati, M. Facile and green synthesis of CuO nanoneedles with high photo catalytic activity. *J. Mater. Sci.: Mater. Electron.* **2016**, *27*, 9454.
(60) Link, S.; El-Sayed, M. A. Optical properties and ultrafast dynamics of metallic nanocrystals. *Annu. Rev. Phys. Chem.* **2003**, *54*, 331−366.
(61) Noginov, M.; Zhu, G.; Bahoura, M.; Adegoke, J.; Small, C.; Ritzo, B.; Drachev, V.; Shalaev, V. M. Enhancement of surface plasmons in an Ag aggregate by optical gain in a dielectric medium. *Opt. Lett.* **2006**, *31*, 3022−3024.
(62) Torres-Rivero, K.; Bastos-Arrieta, J.; Fiol, N.; Florido, A.Chapter Ten - Metal and metal oxide nanoparticles: An integrated perspective of the green synthesis methods by natural products and waste valorization: applications and challenges. In *Comprehensive Analytical Chemistry*; Verma, S. K., Das, A. K., Eds.; vol *94*; Elsevier, 2021; pp 433−469.
(63) Vorobyova, V.; Vasyliev, G.; Pylypenko, I.; Khrokalo, L. Preparation, characterization, and antibacterial properties of "green" synthesis of Ag nanoparticles and AgNPs/kaolin composite. *Appl. Nanosci.* **2022**, *12*, 889−896.
(64) Singla, S.; Jana, A.; Thakur, R.; Kumari, C.; Goyal, S.; Pradhan, J. Green synthesis of silver nanoparticles using Oxalis griffithii extract and assessing their antimicrobial activity. *OpenNano* **2022**, *7*, No. 100047.
(65) Pérez-Marroquín, X. A.; Aguirre-Cruz, G.; Campos-Lozada, G.; Callejas-Quijada, G.; León-López, A.; Campos-Montiel, R. G.; García-Hernández, L.; Méndez-Albores, A.; Vázquez-Durán, A.; Aguirre-Álvarez, G. Green Synthesis of Silver Nanoparticles for Preparation of Gelatin Films with Antimicrobial Activity. *Polymer* **2022**, *14*, 3453.
(66) Pham, T. T. H.; Dien, N. D.; Vu, X. H. Facile synthesis of silver/gold alloy nanoparticles for ultra-sensitive rhodamine B detection. *RSC Adv.* **2021**, *11*, 21475−21488.
(67) Atta, A. M.; Moustafa, Y. M.; Al-Lohedan, H. A.; Ezzat, A. O.; Hashem, A. I. Methylene Blue Catalytic Degradation Using Silver and Magnetite Nanoparticles Functionalized with a Poly(ionic liquid) Based on Quaternized Dialkylethanolamine with 2-Acrylamido-2-methylpropane Sulfonate-co-Vinylpyrrolidone. *ACS Omega* **2020**, *5*, 2829−2842.
(68) Nguyen, H. S.; Nguyen, T. A.; Luu, T. L. A.; Nguyen, T. P.; Nguyen, T. C.; Nguyen, N. P. T.; Nguyen, T. B.; Nguyen, T. T. H.; Nguyen, H. L.; Kim, I. T.; Nguyen, C. T. Ag-decorated novel h'-WO3 nanostructures for sustainable applications. *Ceram. Int.* **2022**, *48*, 18687−18698.
(69) Zenebe, A.; Kabir Ud, D.; Mohammed Yimer, A.; Kuzhunellil, S.; Demissie, H. Green synthesis of magnetic nanocomposite by Cordia Africana (CA) leave extract for the treatment of Methylene blue contaminated water. *Chem. Eng. J. Adv.* **2021**, *8*, No. 100193.
(70) Pluangklang, C.; Rangsriwatananon, K. Facile Method by Bentonite Treated with Heat and Acid to Enhance Pesticide Adsorption. *Appl. Sci.* **2021**, *11*, 5147.
(71) Kumari, S.; Anjitha, V.; Sengupta, S. Adsorptive mitigation of fluoride ions using aluminosilicate adsorbents: A state-of-the-art review. *Environ. Challenges* **2021**, *5*, No. 100329.
(72) Tackie-Otoo, B. N.; Atta, D. Y.; Ayoub Mohammed, M. A.; Otchere, D. A. Investigation into the oil recovery process using an organic alkali−amino acid-based surfactant system. *Energy Fuels* **2021**, *35*, 11171−11192.
(73) Wang, N.; Hu, Y.; Zhang, Z. Sustainable catalytic properties of silver nanoparticles supported montmorillonite for highly efficient recyclable reduction of methylene blue. *Appl. Clay Sci.* **2017**, *150*, 47−55.
(74) Zhu, M.; Nguyen, M. T.; Chau, Y.-T. R.; Deng, L.; Yonezawa, T. Pt/Ag Solid Solution Alloy Nanoparticles in Miscibility Gaps Synthesized by Cosputtering onto Liquid Polymers. *Langmuir* **2021**, *37*, 6096−6105.
(75) He, K.; Chen, N.; Wang, C.; Wei, L.; Jikun, C. Method for Determining Crystal Grain Size by X-Ray Diffraction. *Cryst. Res. Technol.* **2018**, *53*, No. 1700157.
(76) Kumar, B.; Smita, K.; Debut, A.; Cumbal, L. Synthesis and characterization of SnO2 nanoparticles using cochineal dye. *Appl. Phys. A: Mater. Sci. Process.* **2020**, *126*, 779.
(77) Skiba, M.; Vorobyova, V. Green synthesis and characterization of silver nanoparticles using Prunus persica L. (peach pomace) with natural deep eutectic solvent and plasma-liquid process. *Chem. Pap.* **2022**, *76*, 5789−5806.
(78) Zhang, C.; Wang, Y.; Li, S.; Feng, X.; Liu, L.; Wang, Y.; Zhao, L. Electrospinning and Catalytic Properties of Cyclodextrin Functionalized Polyoxymethylene (POM) Nanofibers Supported by Silver Nanoparticles. *Adv. Polym. Technol.* **2021**, *2021*, No. 8272626.

https://doi.org/10.1021/acsomega.2c05265
ACS Omega 2023, 8, 480−491

(79) Joshi, P.; Raturi, A.; Srivastava, M.; Khatri, O. P. Graphene oxide, kaolinite clay and PVA-derived nanocomposite aerogel as a regenerative adsorbent for wastewater treatment applications. *J. Environ. Chem. Eng.* **2022**, *10*, No. 108597.
(80) Kurtan, U.; Baykal, A.; Sözeri, H. Recyclable Fe3O4@ Tween20@ Ag nanocatalyst for catalytic degradation of azo dyes. *J. Inorg. Organomet. Polym. Mater.* **2015**, *25*, 921−929.
(81) Kurtan, U.; Amir, M.; Yıldız, A.; Baykal, A. Synthesis of magnetically recyclable MnFe2O4@ SiO2@ Ag nanocatalyst: its high catalytic performances for azo dyes and nitro compounds reduction. *Appl. Surf. Sci.* **2016**, *376*, 16−25.
(82) Nas, M. S. AgFe2O4/MWCNT nanoparticles as novel catalyst combined adsorption-sonocatalytic for the degradation of methylene blue under ultrasonic irradiation. *J. Environ. Chem. Eng.* **2021**, *9*, No. 105207.
(83) Kebede, W. L.; Kuo, D.-H.; Zeleke, M. A.; Ahmed, K. E. A novel Sb-doped Mo (O, S) 3 oxy-sulfide photocatalyst for degradation of methylene blue dye under visible light irradiation. *J. Alloys Compd.* **2019**, *797*, 986−994.
(84) Noypha, A.; Areerob, Y.; Chanthai, S.; Nuengmatcha, P. Fe2O3-graphene anchored Ag nanocomposite catalyst for enhanced sonocatalytic degradation of methylene blue. *J. Korean Ceram. Soc.* **2021**, *58*, 297−306.

https://doi.org/10.1021/acsomega.2c05265
ACS Omega 2023, 8, 480−491